Astron. Astrophys. 362, 1065–1071 (2000)

ASTRONOMY AND ASTROPHYSICS

The derivation of pulsation velocities from Doppler line profiles in M-type Mira variables

M. Scholz[1,3] **and P.R. Wood**[2]

[1] Institut für Theoretische Astrophysik der Universität Heidelberg, Tiergartenstrasse 15, 69121 Heidelberg, Germany (scholz@ita.uni-heidelberg.de)
[2] Australian National University, Research School of Astronomy and Astrophysics, Private Bag, Weston Creek PO, ACT 2611, Australia (wood@mso.anu.edu.au)
[3] University of Sydney, Chatterton Department of Astronomy, School of Physics, NSW 2006, Australia

Received 12 April 2000 / Accepted 8 September 2000

Abstract. Model atmospheres for pulsating Mira variables have been used to examine the correction factor that should be used to convert radial velocities derived from the Doppler profiles of observed infrared lines into the velocities immediately above and below the strong shock in the atmosphere. The correction factor varies by a moderate amount depending on the lines selected. Correction factors of $\sim$1.25 and 1.4 are appropriate for the conversion of the observed velocities of the outflowing, post-shock and infalling pre-shock material, respectively, when the lines are strong. This is the case for the low excitation CO 1st vibrational overtone lines in the K band. A correction factor of 1.6 or more is appropriate for the weaker lines of OH and the 2nd vibrational overtone of CO in the H band. These results mean that the true pulsation velocity amplitude of a typical Mira variable is $\sim$34 km s^{-1}. Such large pulsation velocity amplitudes are inconsistent with current models for Mira variables pulsating in the first overtone mode but are consistent with pulsation in the fundamental mode.

Key words: line: profiles – stars: atmospheres – stars: late-type – stars: oscillations – stars: variables: general

1. Introduction

The estimation of the true pulsation velocity of a radially pulsating star from the observed Doppler shift of absorption lines in the stellar spectrum requires a conversion factor of order 1.3-1.4 (eg. Parsons 1972 and references therein). In the case of a star such as a Cepheid variable, where velocity gradients in the stellar atmosphere are small at nearly all phases, the conversion factor from observed to true velocity is mostly a geometric one arising from the fact that matter seen by the observer can be moving at any angle between zero (matter at the centre of the disk) and 90^o (matter at the edge of the stellar disk) to the line of sight. Limb darkening contributes further to the purely geometric correction factor.

In the case of Mira variables, calculation of the correction factor is much more complicated. In the first place, the parts of the atmosphere contributing to line formation contain a large velocity gradient which is comparable to the total velocity amplitude. In addition, different wavelength regions sample very different parts of the atmosphere as demonstrated by the fact that the velocities and velocity amplitudes obtained from optical and infrared spectra are very different. The full velocity amplitudes obtained from absorption lines in the optical region are small (about 10 km s^{-1}, Joy 1954) and appear always to be positive with respect to the velocity of the stellar center-of-mass, thus always representing infalling matter (Wood 1979). The optical spectra sample only the upper layers of the pulsating atmosphere where velocities are relatively small. On the other hand, infrared spectra in the H and K bands yield much larger velocity amplitudes (eg. Hinkle 1978) spanning the center-of-mass velocity: the atmospheres of Mira variables are much more transparent in the infrared.

A second complicating factor concerning spectral line formation in Mira variables is the large extension of the atmosphere. In such an atmosphere, the large volumes of matter in the outer layers, although they may emit only weakly per unit volume, can still cause substantial "nebular" emission components to the line profiles, which often have a P-Cygni shape. Because the velocity of the outer layers can be either positive or negative with respect to the deeper layers forming the main absorption line, the P-Cygni-like emission can be on either the blue or red side of the absorption component. Furthermore, matter in the outermost layers is sometimes seen on the far side of the star by the observer so that the same layers may contribute to both red and blue shifted line components. The P-Cygni emission will clearly affect the velocity derived from the absorption component of any line.

In past studies of Mira variables, it has been usual to assume that observed infrared H and K band line velocities can be converted to true pulsational velocities by using a conversion factor of $\sim$1.4 (e.g. Willson 1982; Wood 1987). In this paper, the correction factor appropriate for infrared spectra is evaluated.

Send offprint requests to: M. Scholz

Table 1. Properties of Mira model series

Series	Mode	P(days)	$M/M_\odot$	$R_{\rm p}/R_\odot$	$T_{\rm eff}$	Δv
Z	f	334	1.0	236	3370	36
D	f	330	1.0	236	2900	31
E	o	328	1.0	366	2700	15
P	f	332	1.0	241	2860	40
M	f	332	1.2	260	2750	42
O	o	320	2.0	503	2250	22

R_p is the radius of the static parent star at Rosseland optical depth unity and Δv is the total pulsational velocity amplitude. f and o stand for fundamental and first overtone pulsation, respectively.

Table 2. Typical absorption line properties

Line Type	χ	$\log gf$	$\lambda_0(\mu$m)
CO 1st	0.0	–6	2.32
	0.6	–5	2.32
	1.2	–5	2.32
CO 2nd	0.3	–8	1.62
	0.9	–6	1.62
	1.5	–6	1.62
OH 1st	0.5	–5	1.62
	1.5	–5	1.62

χ is the excitation potential in eV. λ_0 is the assumed rest wavelenth of the line.

2. The pulsation models and line profile calculations

The pulsation models used here are from six model series described in Bessell et al. (1996) and Hofmann et al. (1998). Their basic properties are summarized in Table 1. Limitations and shortcomings of the models are discussed in these two papers and should be kept in mind. In particular, numerical smearing of quantities close to shock front discontinuities in the pulsation models was only partly removed for the line computations. Details of predicted profiles may be affected by an inadequate treatment of the shock region but the positions of the deep-absorption parts of profiles important for converting Doppler positions into pulsation velocities should be reliable.

The presently available atmospheric models cover several phases and pulsation cycles with a time resolution of 0.2 to 0.5 cycles. The most interesting phases are those around maximum when the shock amplitude is largest. It is this maximum value of the shock amplitude that is mostly used for comparison of observations and pulsation models. Further research on the time dependence of spectra, based on a larger number of phase points, is intended in the future.

The principles of line calculation were outlined in Bessell et al. (1996). The stellar disk was divided into about 50 to 100 rings from the centre to the model surface, and the intensity emitted towards the observer was calculated in each ring from Planck source functions. Summing up all rings yields the observable line profile. The contribution from any layer to the intensity depends on the line absorption coefficient (Voigt profile with 2 km s^{-1} depth-independent microturbulent velocity) and the Doppler shift in that layer due to the projected outflow or infall velocity. Near the model surface of very extended configurations, contributions from the star's far side may be noticeable.

The hot post-shock zone is considered as a transparent layer of negligible thickness, so that no emission lines from this layer are considered in the present models. The emission components found in various lines in the current models are solely due to the above-mentioned "nebular" effect. P Cygni type profiles in M-type Miras have been reported for various metallic lines (e.g. Ferlet & Gillet 1984; Gillet et al. 1985a,b) and cannot be readily excluded in the crowded published infrared line spectra (e.g. Hinkle 1978; Hinkle & Barnes 1979).

Our justification for neglecting the shock layer is that detailed models of this layer (e.g. Fox & Wood 1985; Gillet et al. 1989) indicate that it is so thin (typically $< 10^{-3} R_\odot$) compared to the line formation region of a Mira atmosphere (typically $> 10^2 R_\odot$) that its contribution to line optical depths should be negligible. Furthermore, the high temperatures in the post-shock region (>6000K) mean that there will be no molecules there to form the lines that are discussed in this paper. We also note that deviations from our assumed LTE Planck source function resulting from post-shock relaxation should be confined to the thin shock layer and therefore should not be important in the overall line formation process.

Representative CO 1st overtone (Δv = 2), CO 2nd overtone (Δv = 3) and OH (Δv = 2) lines (Table 2) calculated in this study were so chosen that they exhibit typical behaviours in different models. Adopted combinations of excitation potentials and oscillator strengths are rounded values similar to those of lines in the 2.32μm and 1.62μm spectral regions (Hinkle 1978; Smith & Lambert 1985).

3. Results

3.1. Atmospheric velocity structure

We illustrate the typical velocity structure of a Mira atmosphere at various phases by using six D-series models from Bessell et al. (1996). Fig. 1 shows the velocity (positive = outflowing, negative = infalling) plotted against Rosseland optical depth and against radius for these models. The velocity structures are dominated by one or two shock waves that can be seen propagating out from deep in the atmosphere. For the six models in the time series shown here, the first shock to propagate outward is stalled by infalling matter and its position actually moves back inward. In general, below the strong inner shock, matter is outflowing at $\sim$10 km s^{-1} while above the shock material is infalling at $\sim$20 km s^{-1}.

The only well-defined reference velocities in a Mira atmosphere are the velocities immediately below and above the strong inner shock. The aim of this paper is to find the correction factor that needs to be applied to observed velocities (defined in Sect. 3.3) in order to derive the immediate pre- and post-shock velocities.

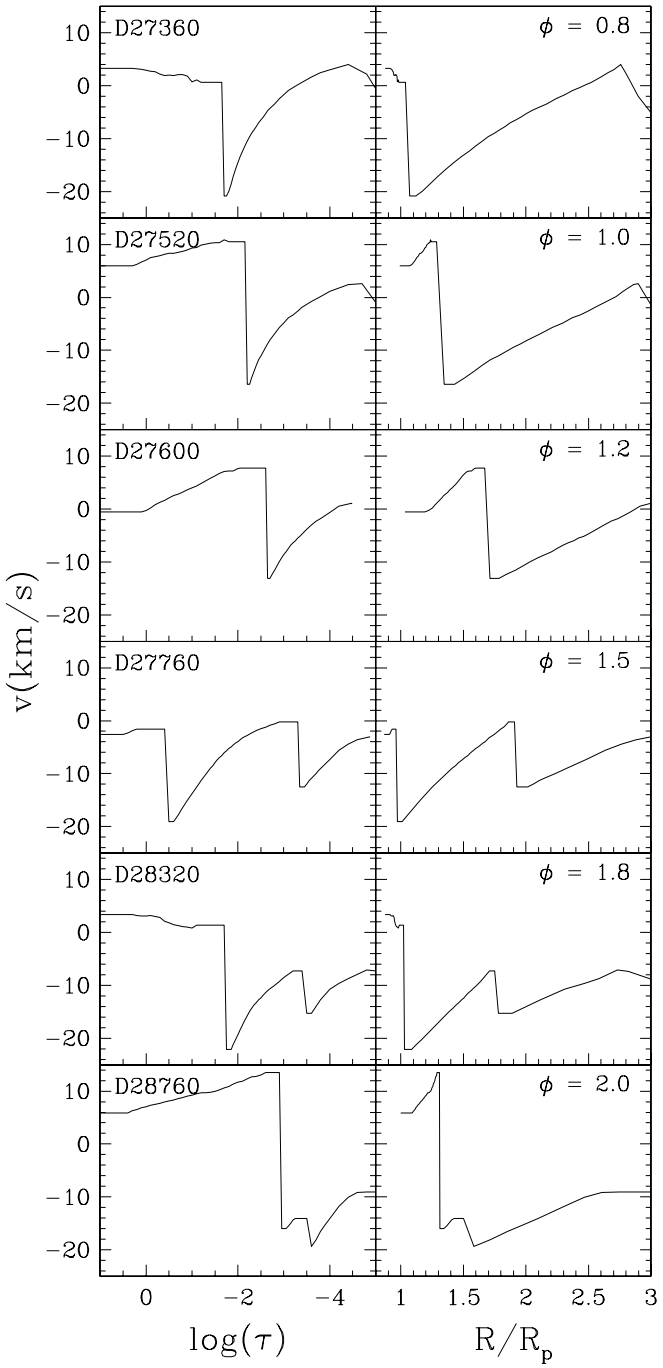

Fig. 1. The velocity in a time series of six Mira models plotted against the Rosseland optical depth τ (left panels) and the radius (right panels). The D-series model number (see Bessell et al. 1996) is indicated on the left panels and the pulsational phase ϕ is given on the right panels. R_p is the Rosseland radius of the static parent star.

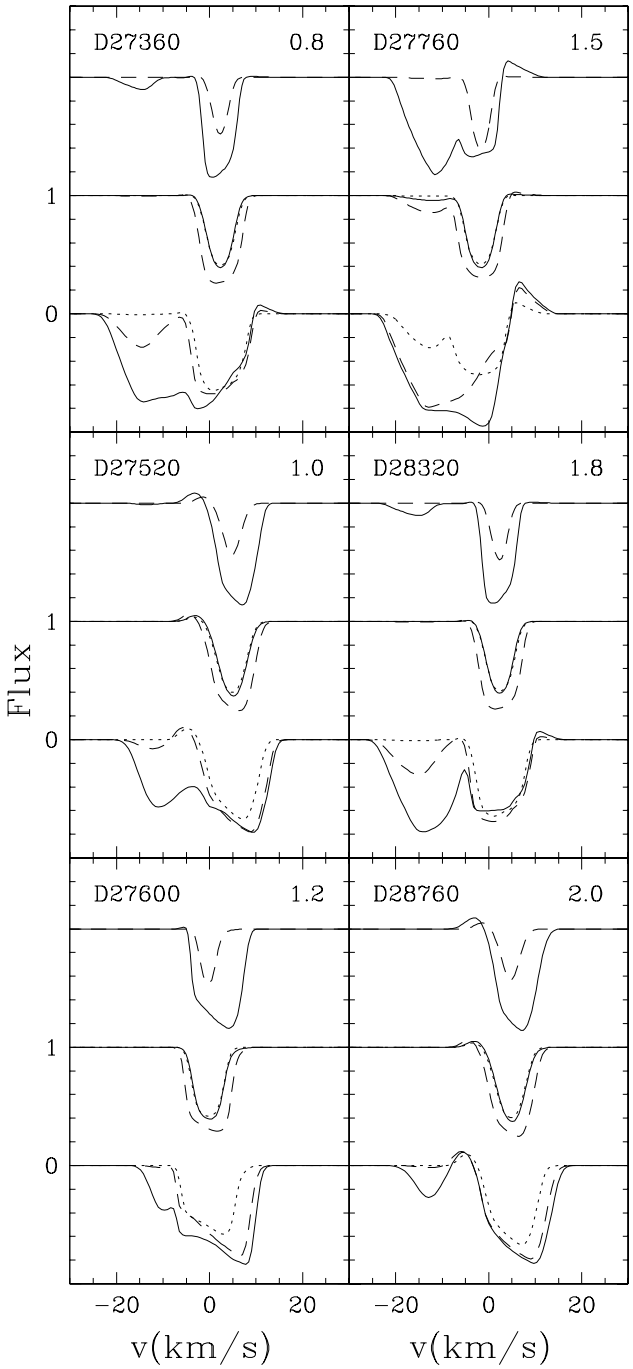

Fig. 2. The flux in various line profiles plotted against velocity, with positive velocity corresponding to motion towards the observer (see text). The model number and its phase is indicated on each panel. The three sets of line profiles in each panel correspond to lines of the CO 1st vibrational overtone (bottom), the CO 2nd vibrational overtone (middle), and of OH (top). The solid, dashed and dotted lines correspond to lines of increasing excitation potential χ, respectively. See Table 2 for the actual values of χ and the corresponding value of $\log gf$.

3.2. Line profiles

In Fig. 2, the flux in various representative (see Table 2) infrared lines is plotted against velocity. For easier comparison with Fig. 1, the velocities are displayed reversed in sign from the traditional spectroscopic Doppler shift, i.e. blue-shifted line components (usually produced by outflowing material seen on the star's near side) are displayed at positive velocities. This convention will be used throughout this paper.

In general, the low excitation, 1st vibrational overtone CO lines are very strong, the low excitation OH lines are next in

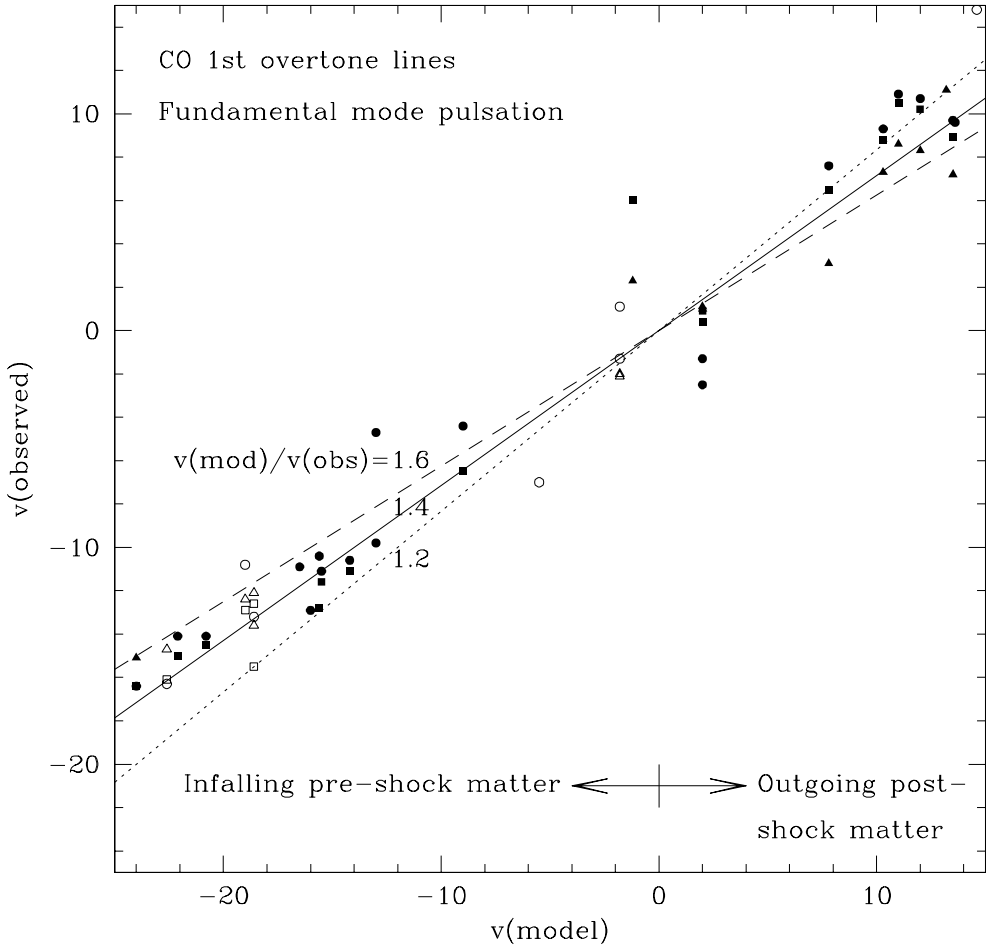

Fig. 3. The observed velocity of CO 1st overtone lines (defined as the velocity at minimum flux in the line, with the sign convention of this paper) plotted against the immediate pre- and post-shock velocities in fundamental mode pulsation models. Solid symbols come from models near maximum ($-0.25 < \phi < +0.25$) while open symbols come from models near minimum ($0.25 < \phi < 0.75$). Circles represent lines with excitation potential 0.0 eV, squares 0.6 eV and triangles 1.2 eV. Lines for three values of the conversion factor from observed to pulsation velocity are also shown.

strength and the 2nd vibrational overtone CO lines are weakest. This general line strength sequence was noted in real Miras by Hinkle (1978). At all times, absorption lines with positive velocities can be seen, these lines being formed in the outflowing material below the strong shock. Before and around maximum, the lower excitation and stronger lines are double, these lines being formed in the both the outflowing post-shock material and the infalling pre-shock material. Because the infalling material is cooler, only the low excitation lines are formed there. Such double lines are seen in the observed infrared spectra of Miras (e.g. Hinkle 1978).

The final point to note in Fig. 2 is the existence of emission components on the edges of various lines as a result of the "nebular" effect noted in the Introduction. These emission components can fall on either the red or blue edges of absorption lines. When lines are double, the emission can fall between the two absorption components.

3.3. Observed velocities versus pre- and post-shock velocities

In order to actually derive a Doppler shift from an observed line, a technique has to be adopted to measure the line velocity. We follow the method of Hinkle and co-workers who use the position of maximum line depth as the line velocity. A program was written to find the minimum in all line profiles automatically, and the velocity was considered observable (and hence stored for plotting) if the central depth relative to the continuum was <0.9.

In Fig. 3, the velocity at line flux minimum in fundamental mode pulsation models is plotted against the velocity of material immediately above and below the main shock wave in the atmosphere. The first point to note is that there is a substantial scatter in the conversion factor f from observed to pulsation velocity. However, for infalling (pre-shock) material, a value $f \approx 1.4$ is generally a good approximation while a lower value of $f \approx 1.25$ seems more appropriate for the outflowing (post-shock) material. The reason for the highly discrepant points is the existence of strong "nebular" emission from the outermost layers of the very extended atmosphere which distorts the absorption line profiles, especially when both pre- and post-shock lines are significant.

Fig. 4 plots the "observed" line velocity against the appropriate model pre- or post-shock velocity for the OH and CO 2nd overtone lines. Here, the required conversion factor of 1.6 or more is larger than for the CO 1st overtone lines, particularly for the warm, outflowing, post-shock matter. The reason for the higher conversion factor for these lines is that they are formed deeper in the star. Because there is usually a significant velocity

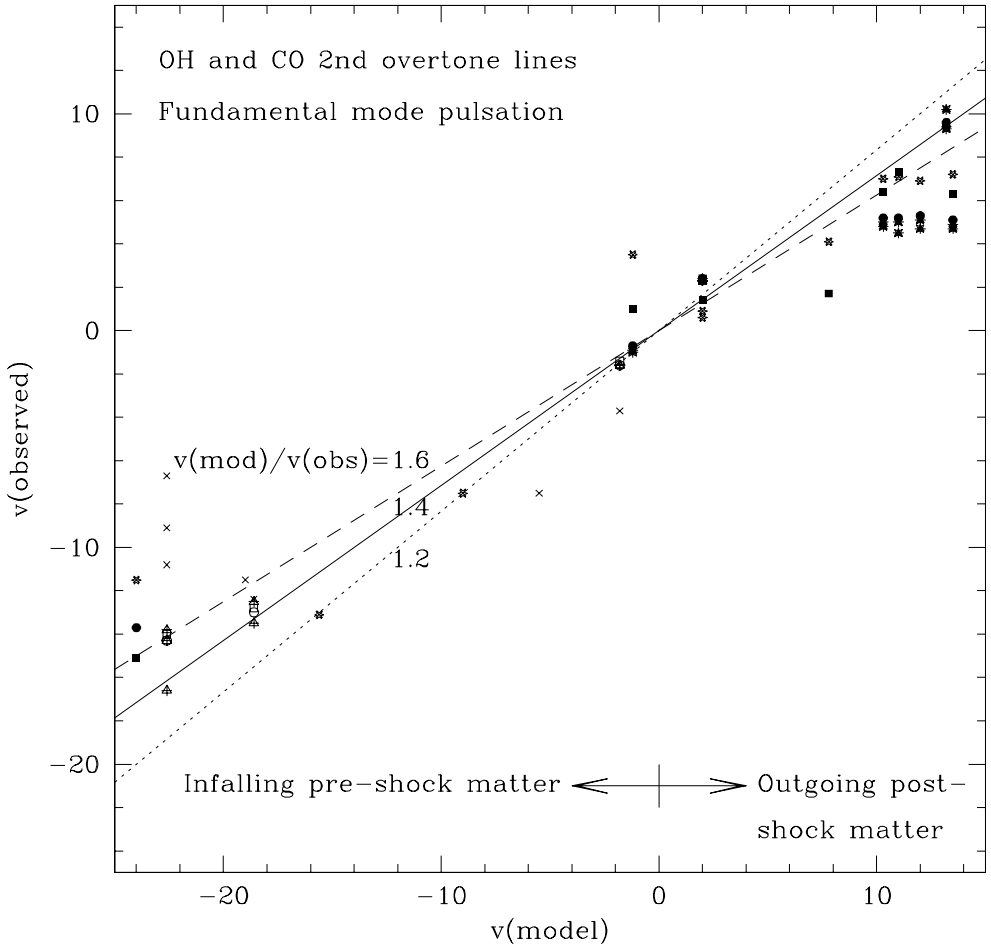

Fig. 4. The observed velocity of OH and CO 2nd overtone lines plotted against the immediate pre- and post-shock velocities. Solid circles, squares and triangles represent CO 2nd overtone lines from models near maximum and with excitation potential 0.3, 0.9 and 1.5 eV, respectively. The corresponding open symbols are from models near minimum. Six and four pointed stars represent OH lines in models near maximum having excitation potentials of 0.5 and 1.5 eV, respectively. Plus signs and crosses represent the corresponding OH lines near minimum. Lines for three values of the conversion factor from observed to pulsation velocity are also shown.

gradient behind the shock front around maximum (Fig. 1), the main region of line formation is expanding at a smaller velocity than is the immediate post-shock region.

Figs. 5 and 6 show the observed and model velocities for first overtone pulsation models. The CO 1st overtone lines show a large scatter with a value of ∼1.2 being appropriate for the conversion factor from observed to pulsation velocity. The CO 2nd overtone and OH lines require a larger conversion factor of ∼1.6. The larger conversion factor for the CO 2nd overtone and OH lines is as expected (see the previous paragraph).

The results above assume a microturbulent velocity v_{turb} of 2 km s^{-1}. In fact, very little is known about microturbulence in Miras because Doppler profiles are so strongly dominated by macroscopic outflow and infall velocities that deriving v_{turb} from line shapes is impossible. Furthermore, curves of growth are not suited for straight-forward interpretation in terms of microturbulent broadening (cf. Scholz 1992). Two additional complications are that v_{turb} possibly depends on depth and on phase, the latter being found in RR Lyrae and δ Cephei variables by Fokin et al. (1999) and Gillet et al. (1999).

For non-Mira M giants, depth-independent microturbulent velocities reported by Harris & Lambert (1984) and Smith & Lambert (1985, 1990) range from 1.6 to 2.9 km s^{-1} with a most typical value slightly above 2 km s^{-1}. Tsuji (1986, 1991) found systematically higher microturbulent velocities ranging from 2.7 to 4.0 km s^{-1} and discussed evidence of depth-dependence, anisotropy and an additional macroturbulent broadening component. Recent model atmospheres of non-Miras using modern opacity sampling data (Plez 1992; Plez et al. 1992; Fluks et al. 1994) use v_{turb} = 2 km s^{-1}. In view of these factors, we adopted a 2 km s^{-1} depth-independent microtubulence for our line profiles. As a check on the robustness of our results we also performed test calculations for the CO 1st overtone lines with v_{turb} = 0 and 4 km s^{-1}. For infalling matter, these calculations produced conversion factors that were not significantly different from those with v_{turb} = 2 km s^{-1}. For outflowing (post-shock) matter, however, the test calculations suggest that the conversion factor decreases with increasing microturbulent velocity so that it should be more like 1.05 when v_{turb} = 4 km s^{-1} rather than the value of ∼1.25 derived for v_{turb} = 2 km s^{-1}. If microturbulent velocities are indeed as large as 4 km s^{-1} in Mira atmospheres, interpretation of line profiles in terms of pulsation velocities will require a thorough investigation of microturbulent line broadening, including possible deviations from the conventional, simple, depth-independent, isotropic, microturbulence concept.

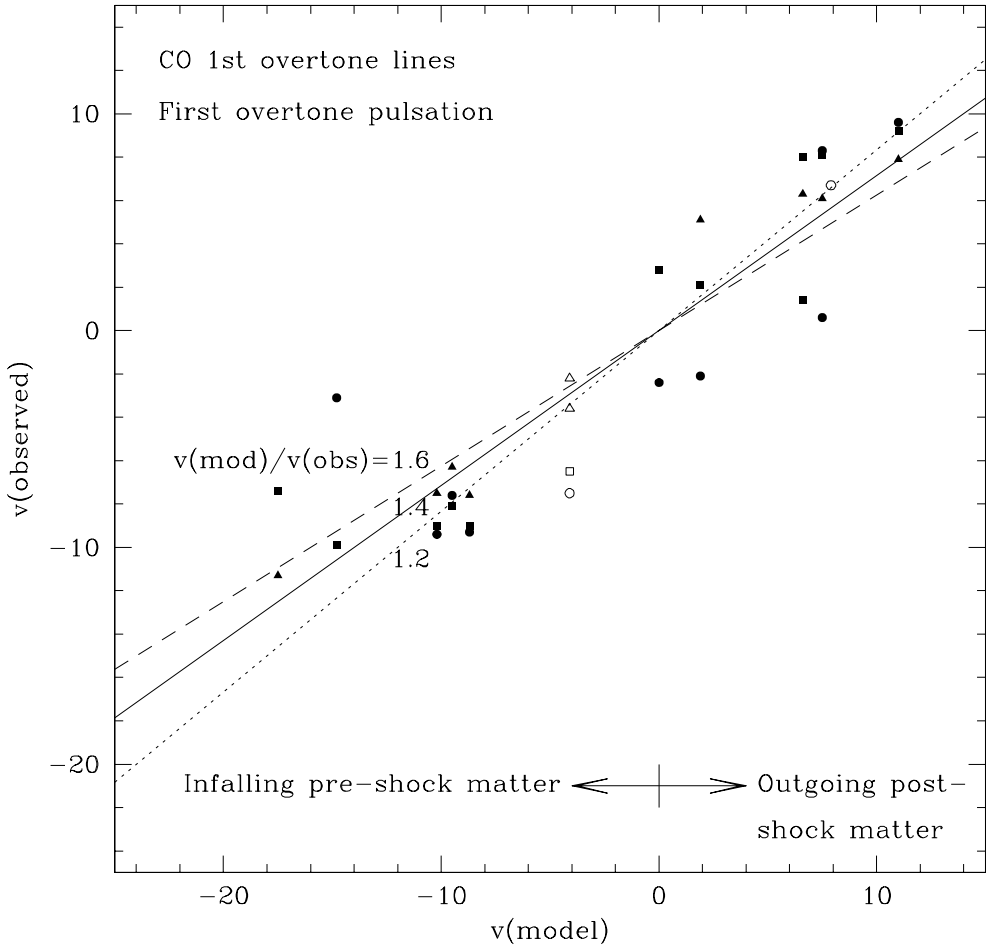

Fig. 5. The same as Fig. 3, but for first overtone pulsation models.

4. Discussion

The conversion factor from observed velocity to pre- and post-shock velocities varies with the line excitation potential and intrinsic strength. For the strongest lines, the results for the 1st overtone CO lines suggest a conversion factor of ∼1.4 for infalling, pre-shock material and ∼1.25 for the outflowing, post-shock material. Larger conversion factors may be appropriate for the outflowing material when weaker lines are used.

The observed, uncorrected infrared velocities of a typical Mira variable can be obtained from Hinkle (1978) and Hinkle et al. (1982; 1984). These velocities have been converted to center-of-mass velocities by Wood (1987) and they show that the typical maximum observed outward velocity is ∼11 km s^{-1} while the typical maximum observed infall velocity is ∼14 km s^{-1}. Taking the conversion factors of 1.25 and 1.4, respectively, as appropriate, a typical Mira variable is seen to have a true post-shock outflow velocity of ∼14 km s^{-1}, a pre-shock infall velocity of ∼20 km s^{-1} and a full velocity amplitude of ∼34 km s^{-1}.

One of the main reasons for considering Mira variables to be fundamental mode rather than first overtone pulsators has been that the observed pulsational velocity amplitudes were larger than could be produced by first overtone pulsators (Bowen 1988; Bessell et al. 1996). However, in the past, the estimation of the true velocity amplitude has involved a guess at the value of the conversion factor from observed to pulsation velocity. The conversion factors found in the present paper confirm that Miras do indeed have true pulsation velocity amplitudes that are too large to be consistent with first overtone pulsation and that the Miras must therefore be fundamental mode pulsators. This statement remains true even if one uses the somewhat uncertain correction factor of ∼1.2 derived from the CO 1st overtone lines in first overtone pulsation models, in which case the pulsation amplitude is 30 km s^{-1} rather than 34 km s^{-1}. Similarly, the adoption of a microturbulent velocity as high as 4 km s^{-1} (see Sect. 3.3) would not significantly affect our conclusion that the Miras must be fundamental mode pulsators. A completely independent identification of the fundamental mode as the pulsation mode in Mira variables has recently been made by Wood et al. (1999) using MACHO observations of long-period variables in the LMC. A remaining unsettled question is why, with a few exceptions, the observed period-radius relation of M-type Miras strongly indicates first-overtone pulsation (e.g. Haniff et al. 1995; van Belle et al. 1996; van Leeuwen et al. 1997).

Acknowledgements. We thank the referee for useful comments and suggestions. M.S. wishes to thank the members of the Chatterton Department of Astronomy, University of Sydney for their hospitality during a research visit in February to April 2000.

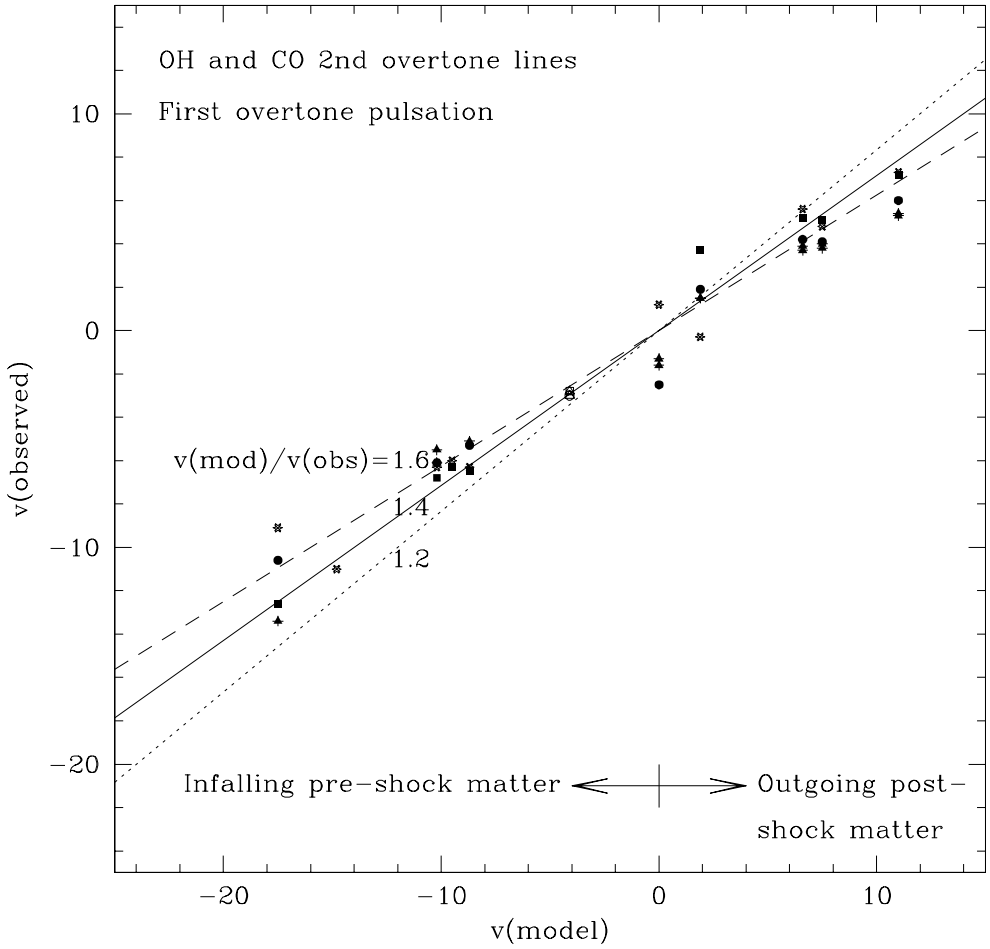

Fig. 6. The same as Fig. 4, but for first overtone pulsation models.

References

Bessell M.S., Scholz M., Wood P.R., 1996, A&A 307, 481
Bowen G.H., 1988, ApJ 329, 299
Ferlet R., Gillet D., 1984, A&A 133, L1
Fluks M.A., Plez B., The P.S., et al., 1994, A&AS 105, 311
Fokin A.B., Gillet D., Chadid M., 1999, A&A 344, 930
Fox M.W., Wood P.R., 1985, ApJ 297, 455
Gillet D., Ferlet R., Maurice E., Bouchet P., 1985a, A&A 150, 89
Gillet D., Fokin A.B., Breitfellner M.G., Mazauric S., Nicolas A., 1999, A&A 344, 935
Gillet D., Lafon J.-P.J., David P., 1989, A&A 220, 185
Gillet D., Maurice E., Bouchet P., Ferlet R., 1985b, A&A 148, 155
Haniff C.A., Scholz M., Tuthill P.G., 1995, MNRAS 276, 400
Harris M.J., Lambert D.L., 1984, ApJ 285, 674
Hinkle K.H., 1978, ApJ 220, 210
Hinkle K.H., Barnes T.G., 1979, ApJ 227, 923
Hinkle K.H., Hall D.N.B., Ridgway S.T., 1982, ApJ 252, 697
Hinkle K.H., Scharlach W.W.G., Hall D.N.B., 1984, ApJS 56, 1
Hofmann K.-H., Scholz M., Wood P.R., 1998, A&A 339, 846
Joy A.H., 1954, ApJS 1, 39
Parsons S.B., 1972, ApJ 174, 57
Plez B., 1992, A&AS 94, 527
Plez B., Brett J.M., Nordlund A., 1992, A&A 256, 551
Scholz M., 1992, A&A 253, 203
Smith V.V., Lambert D.L., 1985, ApJ 294, 326
Smith V.V., Lambert D.L., 1990, ApJS 72, 387
Tsuji T., 1986, A&A 156, 8
Tsuji T., 1991, A&A 245, 203
van Belle G.T., Dyck H.M., Benson J.A., Lacasse M.G., 1996, AJ 112, 2147
Van Leeuwen F., Feast M.W., Whitelock P.A., Yudin B., 1997, MNRAS 287, 955
Willson L.A., 1982, In: Cox J.P., Hansen C.J. (eds.) Pulsations in Classical and Cataclysmic Variable Stars. Joint Institute for Laboratory Astrophysics, Boulder, p. 269
Wood P.R., 1979, ApJ 227, 220
Wood P.R., 1987, In: Cox A.N., Sparks W.M., Starrfield S.G. (eds.) Stellar Pulsation. Lecture Notes in Physics 274, Springer, p. 250
Wood P.R., MACHO collaboration, 1999, In: Le Bertre T., Lèbre A., Waelkens C. (eds.) IAU Symposium 191, Asymptotic Giant Branch Stars. ASP, San Francisco, p. 151